

Graph approximation and generalized Tikhonov regularization for signal deblurring

Davide Bianchi

dept. of Science and High Technology

University of Insubria

Como, Italy

d.bianchi9@uninsubria.it

Marco Donatelli

dept. of Science and High Technology

University of Insubria

Como, Italy

marco.donatelli@uninsubria.it

Abstract—Given a compact linear operator \mathcal{K} , the (pseudo) inverse \mathcal{K}^\dagger is usually substituted by a family of regularizing operators \mathcal{R}_α which depends on \mathcal{K} itself. Naturally, in the actual computation we are forced to approximate the true continuous operator \mathcal{K} with a discrete operator $\mathcal{K}^{(n)}$ characterized by a finesses discretization parameter n , and obtaining then a discretized family of regularizing operators $\mathcal{R}_\alpha^{(n)}$. In general, the numerical scheme applied to discretize \mathcal{K} does not preserve, asymptotically, the full spectrum of \mathcal{K} . In the context of a generalized Tikhonov-type regularization, we show that a graph-based approximation scheme that guarantees, asymptotically, a zero maximum relative spectral error can significantly improve the approximated solutions given by $\mathcal{R}_\alpha^{(n)}$. This approach is combined with a graph based regularization technique with respect to the penalty term.

Index Terms—generalized Tikhonov, graph Laplacian, graph approximation.

I. INTRODUCTION

The aim of this work is to provide a first glimpse about the applications of a full graph-based approximation approach to inverse problems regularization. Since the theory involved can be rather technical and very vast, to keep this manuscript short and almost self-contained, we will mainly concentrate on numerical examples in the one dimensional case.

That said, the model equation we consider is

$$\mathcal{K}[f] = g, \quad (1)$$

where $\mathcal{K} : L^2([0,1]) \rightarrow L^2([0,1])$ is a compact linear operator acting on the Hilbert space of square integrable functions over $[0,1]$. In particular, \mathcal{K} will be the Green operator of a self-adjoint second-order differential operator \mathcal{L} with formal equation

$$\mathcal{L}[g](x) := -g''(x) + q(x)g(x) \quad \forall x \in (0,1).$$

Indicating with \mathcal{K}^\dagger the generalized Moore-Penrose inverse of \mathcal{K} , the solution for the model problem (1) of minimal norm reads $f^\dagger = \mathcal{K}^\dagger g$. It is known that (1) is an ill-conditioned problem, that is, even small errors in the observed data g will greatly affect the reconstructed solution.

We are interested to approximate the solution f^\dagger when only a noisy approximation $g^\epsilon := g + \eta$ is available, with

$$\|g^\epsilon - g\| = \|\eta\| = \epsilon,$$

Supported by INdAM-GNAMPA and INdAM-GNCS.

and where ϵ is called the *noise level*. Since $\mathcal{K}^\dagger g^\epsilon$ is not a good approximation of f^\dagger due to the ill-conditioning of \mathcal{K} , it is commonly chosen to approximate f^\dagger with $f_\alpha^\epsilon := \mathcal{R}_\alpha[g^\epsilon]$, where $\{\mathcal{R}_\alpha\}_{\alpha \in (0,+\infty)}$ is a family of continuous operators depending on a parameter α such that $\mathcal{R}_\alpha \rightarrow \mathcal{K}^\dagger$ pointwise as $\alpha = \alpha(\epsilon) \rightarrow 0$. A classical example is the generalized Tikhonov regularization method defined by

$$\mathcal{R}_\alpha : L^2([0,1]) \rightarrow \text{dom}(\mathcal{A}) \subseteq L^2([0,1]) \quad \text{such that} \quad (2a)$$

$$\mathcal{R}_\alpha[g^\epsilon] := \operatorname{argmin}_{f \in \text{dom}(\mathcal{A})} \left\{ \|\mathcal{K}[f] - g^\epsilon\|^2 + \alpha \|\mathcal{A}[f]\|^2 \right\}, \quad (2b)$$

where $\mathcal{A} : \text{dom}(\mathcal{A}) \subseteq L^2([0,1]) \rightarrow L^2([0,1])$ is a closed and densely defined linear operator such that

$$\ker(\mathcal{A}) < \infty, \quad \ker(\mathcal{A}) \cap \ker(\mathcal{K}) = \{0\}.$$

\mathcal{R}_α is called *generalized Tikhonov regularization operator* and we will write $f_\alpha^\epsilon := \mathcal{R}_\alpha[g^\epsilon]$ for the regularized solution corresponding to the given data g^ϵ . For a detailed account over this topic we refer to [9], [13]. For $\mathcal{A} = \mathcal{I}$, where \mathcal{I} is the identity map, then we recover the standard Tikhonov regularization. The operator \mathcal{A} is typically introduced to force the regularized solution f_α^ϵ to live in $\text{dom}(\mathcal{A})$, whenever we have a-priori informations on particular features of the true solution f^\dagger .

To better understand the role of \mathcal{A} and to help us to simplify the computations, let us make the following, momentarily, assumptions: \mathcal{A} is self-adjoint (with purely discrete spectrum) and it shares the same eigenbase with \mathcal{K} . Indicating with $\{\lambda_m; u_m, v_m\}_{m \in \mathbb{N}}$, $\{\mu_m; u_m, v_m\}_{m \in \mathbb{N}}$ the spectral decomposition of \mathcal{K} and \mathcal{A} , respectively, we can then express the regularized solution f_α^ϵ as

$$f_\alpha^\epsilon = \sum_{m \in \mathbb{N}} \frac{\lambda_m}{\lambda_m^2 + \alpha \mu_m^2} \langle g^\epsilon, u_m \rangle u_m.$$

If $\ker(\mathcal{A}) \neq \{0\}$, then we can write

$$f_\alpha^\epsilon = \sum_{u_m \in \ker(\mathcal{A})} \lambda_m^{-1} \langle g^\epsilon, u_m \rangle u_m + \sum_{u_m \notin \ker(\mathcal{A})} \frac{\lambda_m}{\lambda_m^2 + \alpha \mu_m^2} \langle g^\epsilon, u_m \rangle u_m.$$

The above equation tells that the regularized solution f_α^ϵ is made of the sum of two parts: the first part is the projection of the observed data g^ϵ into $\ker(\mathcal{A})$ and no regularization takes action since α does not play any role in it, and the second part is the remainder of the summation where instead the regularization operator takes action. Writing $F_\alpha(t) := \frac{t^2}{t^2 + \alpha}$, and

$$\begin{aligned} \mathbf{err}_{app,\perp} &:= - \sum_{u_m \notin \ker(\mathcal{A})} \left(1 - F_\alpha\left(\frac{\lambda_m}{\mu_m}\right)\right) \lambda_m^{-1} \langle g, u_m \rangle u_m, \\ \mathbf{err}_{noise,\perp} &:= \sum_{u_m \notin \ker(\mathcal{A})} F_\alpha\left(\frac{\lambda_m}{\mu_m}\right) \lambda_m^{-1} \langle \eta, u_m \rangle u_m, \end{aligned}$$

then

$$\begin{aligned} \|f_\alpha^\epsilon - f^\dagger\| &= \|f_\alpha^\epsilon - f^\dagger\|_{\ker(\mathcal{A})} + \|f_\alpha^\epsilon - f^\dagger\|_{\ker(\mathcal{A})^\perp} \\ &= \left\| \sum_{u_m \in \ker(\mathcal{A})} \lambda_m^{-1} (\langle g^\epsilon, u_m \rangle u_m - \langle g, u_m \rangle u_m) \right\| \\ &\quad + \|\mathbf{err}_{app,\perp} + \mathbf{err}_{noise,\perp}\| \\ &= \left\| \sum_{u_m \in \ker(\mathcal{A})} \lambda_m^{-1} \langle \eta, u_m \rangle u_m \right\| \\ &\quad + \|\mathbf{err}_{app,\perp} + \mathbf{err}_{noise,\perp}\| \\ &\leq c\epsilon + \|\mathbf{err}_{app,\perp} + \mathbf{err}_{noise,\perp}\|, \end{aligned}$$

where $c = \max\{\lambda_m^{-1} : u_m \in \ker(\mathcal{A})\}$. So, if f^\dagger belongs entirely to $\ker(\mathcal{A})$, the best possible strategy would be to just project f_α^ϵ onto the kernel of \mathcal{A} , such that to delete the error coming from $\mathbf{err}_{app,\perp}$ and $\mathbf{err}_{noise,\perp}$. Morally speaking, when choosing the operator \mathcal{A} we should look that as much features as possible of f^\dagger belong to $\ker(\mathcal{A})$. For example, a typical choice for \mathcal{A} in imaging is the Laplace operator with Dirichlet or Neumann boundary conditions: the first one is chosen when dealing with astronomical images that have a black background, which correspond to a zero numeric value at the boundary of the field of view, in the grayscale representation; the second one is chosen because images have several areas of homogeneous, constant color. For a reference, see [1]. Clearly, in the real applications it is not usually granted that \mathcal{K} and \mathcal{A} commute, and in some works it was proposed to use $\mathcal{A} = F(\mathcal{K}\mathcal{K}^*)$, where F is a suitable function on the spectrum of $\mathcal{K}\mathcal{K}^*$ that mimic the spectral distribution of the Laplace operator, see [4], [15], [18].

In the actual computations we can not make use of the continuous operator \mathcal{K} and \mathcal{A} , but only of discrete approximations $\mathcal{K}^{(n)}$ and $\mathcal{A}^{(n)}$, respectively, that are obtained by numerical discretization schemes. As a consequence, the ideal family of regularization operators $\{\mathcal{R}_\alpha\}_\alpha$ is substituted by a family of discrete operators $\{\mathcal{R}_\alpha^{(n)}\}_\alpha$, such that

$$\mathcal{R}_\alpha^{(n)}[g_n^\epsilon] := \operatorname{argmin}_{f_n \in L_n} \left\{ \|\mathcal{K}^{(n)}[f_n] - g_n^\epsilon\|^2 + \alpha \|\mathcal{A}^{(n)}[f_n]\|^2 \right\}, \quad (3)$$

where L_n is a finite dimensional space that approximates $L^2([0, 1])$. Clearly, the discrete approximation can introduce

extra round-off errors, part of which comes from a bad approximation of the full spectrum of \mathcal{K} . The idea is that if we can have a better control on the spectral relative error, we can obtain a better regularized solution.

This paper is organized as follows: in Section II we report some notations from graph theory. In Section III we show a graph based approximation method to obtain a discretized operator such that it preserves uniformly the original spectrum of \mathcal{K} . We will see that the key point is to use the Fourier coefficients of the inverse Weyl distribution function associated to \mathcal{K} (or, equivalently, to \mathcal{L}) as weights of a transformed-path graph Laplacian. In Section IV, we build the operator \mathcal{A} in the penalty term as the graph Laplacian associated to a given graph G . The main idea is to encode in \mathcal{A} informations from the observed data g^ϵ that can help to better define the space where to force into the regularized solution. Finally, in Section V we provide some numerical examples.

II. GRAPH SETTING

Given a countable set of nodes $X = \{x_i : i \in I\}$, a graph G on X is a pair (w, κ) such that

- $w : X \times X \rightarrow [0, \infty)$ is a nonnegative, symmetric function with zero diagonal;
- $\kappa : X \rightarrow [c, \infty)$ is a lower-bounded function, $c > -\infty$.

In a more compact notation, we write $G = (X, w, \kappa)$, and whenever $\kappa \equiv 0$ we will just write $G = (X, w)$. k is called *potential* (or *killing*) term. For a detailed modern introduction to graph theory, see [17]. Every unordered pair of nodes $e = \{x_i, x_j\}$ such that $w(x_i, x_j) > 0$ is called *edge* incident to x_i and to x_j , and the collection E of all the edges is uniquely determined by w . The non-zero values $w(x_i, x_j)$ are called *weights* associated with the edges $\{x_i, x_j\}$, and w is the *edge-weight* function. Two nodes x_i, x_j are said to be *neighbors* (or *connected*) in G if $\{x_i, x_j\}$ is an edge and we write $x_i \sim x_j$. In this work, we will assume that X is endowed with the counting measure and that every node x_i is connected at most with a finite number of nodes x_j . The sum of all the weights incident to a node x_i is called the *degree* of x_i . In the case that $w(x_i, x_j) \in \{0, 1\}$, then G is said to be *unweighted*. Given a real valued function f on X , the (formal) *graph Laplacian* Δ of G applied to f is defined via

$$\Delta[f](x_i) := \sum_{x_j \in X} w(x_i, x_j) (f(x_i) - f(x_j)) + \kappa(x_i) f(x_i). \quad (4)$$

For a *connected* graph, that is, a graph where for every pair $\{x_i, x_j\}$ there exists a sequence of connected nodes such that $x_i = x_{i_0} \sim \dots \sim x_{i_k} = x_j$, the *combinatorial* distance function $d : X \times X \rightarrow [0, \infty)$ reads as

$$d(x_i, x_j) := \min\{k \in \mathbb{N} : x_i = x_{i_0} \sim x_{i_1} \sim \dots \sim x_{i_k} = x_j\},$$

and $d_\infty := \max\{d(x_i, x_j) : x_i, x_j \in X\}$ is the *combinatorial diameter* of G . Given an unweighted graph $G = (X, w)$ and a proper subset $X_0 \subset X$, we call *Dirichlet m -path graph*

Laplacian, associated to X_0 and G , the operator $\Delta_{k,\text{dir}}$ defined by

$$\Delta_{m,\text{dir}}[f](x_i) := \sum_{\substack{x_j \in X_0: \\ d(x_i, x_j) = m}} (f(x_i) - f(x_j)) + \kappa_{m,\text{dir}}(x_i) f(x_i), \quad (5)$$

where

$$\kappa_{m,\text{dir}}(x_i) := \sum_{x_j \in X \setminus X_0} \mathbb{1}_{\{k\}}(d(x_i, x_j))$$

and

$$\mathbb{1}_{\{k\}}(t) := \begin{cases} 1 & \text{if } t = k, \\ 0 & \text{otherwise.} \end{cases}$$

We call $\kappa_{m,\text{dir}}(\cdot)$ the *Dirichlet boundary potential*. Finally, given a function $\phi : \mathbb{N} \rightarrow \mathbb{R}$, we define the *Dirichlet transformed-path graph Laplacian* $\Delta_{\infty,\text{dir}}$ as

$$\Delta_{\infty,\text{dir}} := \sum_{m=1}^{d_\infty} \phi(m) \Delta_{m,\text{dir}}. \quad (6)$$

About (5) and (6), they are a slight generalization of the original definitions of m -path graph Laplacian and the transformed-path graph Laplacian, respectively, which can be found in [10], [11]. Those generalizations take into account the potential term $\kappa_{m,\text{dir}}$ that counts the edge deficiency of a node in X_0 with respect to its degree value as a node in X , the node-set of the original graph G , see [16] and [2, Section 7.1] for an example of graph discretization of a PDE by Dirichlet subgraphs.

III. GRAPH APPROXIMATION OF \mathcal{K}

Making a simplification, when discretizing problem (1) we pass from the continuous operator \mathcal{K} to a (matrix) discrete operator $\mathcal{K}^{(n)}$ which acts on a finite dimensional space L_n , isomorph to \mathbb{R}^n , such that $L_n \subset L_{n+1} \subset \dots \subset L^2([0, 1])$ and $\bigcup_{n=1}^{\infty} L_n = L^2([0, 1])$. For a detailed account about regularization methods by projection, we point the interested reader to [9, Section 5.2], and all the references therein.

The discrete operator $\mathcal{K}^{(n)}$ has to be consistent with \mathcal{K} and, therefore, at least it has to satisfy

- (P1) $\|\mathcal{K}^{(n)}[f_n] - \mathcal{K}[f]\| \rightarrow 0$ as $n \rightarrow \infty$, where f_n is the projection of f into L_n and $\|\cdot\|$, in this case, can be both the L^2 norm or the sup norm;
- (P2) $\left| \frac{\lambda_m^{(n)}}{\lambda_m} - 1 \right| \rightarrow 0$ as $n \rightarrow \infty$, for every fixed $m \in \mathbb{N}$, where $\lambda_m^{(n)}$ and λ_m are the eigenvalues of the discretized operator $\mathcal{K}^{(n)}$ and of the continuous operator \mathcal{K} , respectively.

It often happens that estimate (P2) does not work on all the spectrum, that is, if $m = m(n)$ is not fixed then (P2) is not satisfied. We call *local spectral relative error* (LSRE) the numerical quantity in (P2). Writing

$$\mathcal{E} := \limsup_{n \rightarrow \infty} \max_{m=1, \dots, n} \left\{ \left| \frac{\lambda_m^{(n)}}{\lambda_m} - 1 \right| \right\}, \quad (7)$$

the preceding remark translates into saying that, in general, $\mathcal{E} > 0$. Clearly, this introduces more errors in the regularization process. We call \mathcal{E} the *maximum spectral relative error*

(MSRE), see [3] for more details. We want to show that, if we can guarantee

(P2') $\mathcal{E} = 0$,

then we obtain a significant improvement in the approximation of the regularized solution f_n^ϵ . For simplicity, suppose that \mathcal{K} is a compact linear operator such that

$$\mathcal{K}[f](x) := \int_0^1 h(x, y) f(y) dy \quad (8)$$

whose kernel h is the Green function of the following second-order differential operator $\mathcal{L} : \text{dom}(\mathcal{L}) \subset L^2([0, 1]) \rightarrow L^2([0, 1])$,

$$\begin{cases} \text{dom}(\mathcal{L}) := H_0^1([0, 1]), \\ \mathcal{L}[g](x) := -g''(x) + q(x)g(x), \end{cases} \quad (9)$$

where we suppose q to be bounded, and H_0^1 is the usual closure of the set of compactly supported smooth functions $C_c^\infty(0, 1)$ with respect to the Sobolev space H^1 . In other words, \mathcal{L} is a Schrödinger-type operator with Dirichlet boundary conditions (BCs). We suggest the following readings about this topic, [6], [12]. We can think of \mathcal{K} as the pseudo-inverse of \mathcal{L} , i.e., $\mathcal{K} = \mathcal{L}^\dagger$. Therefore, if we find a way to discretize \mathcal{L} such that the MSRE associated to the discretization of \mathcal{L} is zero, i.e., such that $\mathcal{E} = \mathcal{E}(\mathcal{L}) = 0$, then we will have that the MSRE associated to the discretization of \mathcal{K} will be zero, i.e., $\mathcal{E} = \mathcal{E}(\mathcal{K}) = 0$, by the substitution $\mathcal{K}^{(n)} = \mathcal{L}^{(n)\dagger}$.

For this regard, let $G = (X, w)$ be such that

- $X = \left\{ x_i = \frac{i}{n+1} : i \in \mathbb{Z} \right\}$;
- $w(x_i, x_j) = \begin{cases} 1 & \text{if } |i - j| = 1, \\ 0 & \text{otherwise.} \end{cases}$

Fix $n \in \mathbb{N}$, define $X^{(n)} := X \cap (0, 1)$ and set the Dirichlet transformed-path graph Laplacian $\Delta_{\infty,\text{dir}}$, associated to $X^{(n)}$ and G , with

$$\phi(m) := (-1)^{m+1} \frac{2}{m^2}.$$

The choice of ϕ is not random. Indeed, $\sum_{m \geq 1} \phi(k) = -\pi^2/3$ and $\{\pi^2/3\} \cup \{-\phi(m)\}_{m \in \mathbb{N}}$ are the Fourier coefficients of $\zeta(\theta) = \theta^2$ over the interval $[0, \pi]$, and the inverse Weyl distribution function of the operator \mathcal{L} in (9) is exactly given by ζ . Now, let us observe that $d_\infty = \infty$ and that $\Delta_{m,\text{dir}} = 2I_n$ for every $m > n$, where I_n is the identity matrix $n \times n$. It is not difficult to prove then that $\Delta_{\infty,\text{dir}}$ is well-defined, and in particular let us observe that it is a symmetric Toeplitz matrix $n \times n$ whose stencil \mathbf{t} is given by

$$\mathbf{t} = \left[\frac{\pi^2}{3}, -2, \dots, (-1)^n \frac{2}{n^2} \right]. \quad (10)$$

This last remark will play a crucial role, as we will see shortly. For a review about Toeplitz matrices and their spectra, we refer to [7]. Finally, let us define the operator $\mathcal{L}^{(n)}$ via

$$\mathcal{L}^{(n)} := n^2 \Delta_{\infty,\text{dir}} + Q^{(n)},$$

where $Q^{(n)}$ is the $n \times n$ diagonal matrix whose entries are given by the pointwise evaluation of q over $X^{(n)}$. It is a

fact that $\mathcal{L}^{(n)}$ approximates \mathcal{L} over $C_c^\infty(0,1)$, and it can be checked by two different approaches. Indeed, the stencil \mathbf{t} can be obtained by both the sinc collocation method, see [19], and as a limit of the $(2p+1)$ -points Finite Difference method, where $p \rightarrow \infty$, see [3]. If we now write $\delta_m^{(n)}$ and δ_m for the m -th eigenvalue of $\mathcal{L}^{(n)}$ and \mathcal{L} , respectively, then we obtain that

$$\limsup_{n \rightarrow \infty} \max_{m=1, \dots, n} \left\{ \left| \frac{\delta_m^{(n)}}{\delta_m} - 1 \right| \right\} = 0,$$

that is, $\mathcal{E}(\mathcal{L}) = 0$. This is due to this specific discretization and the stencil \mathbf{t} , since $\zeta(\theta) = \theta^2$ is exactly the (inverse) Weyl distribution function associated to \mathcal{L} , as we observed earlier. We do not get into the details here, for some references see [3, Section 3.2].

We can now define

$$\mathcal{K}^{(n)} := \mathcal{L}^{(n)\dagger}, \quad (11)$$

see Algorithm 1. The operator $\mathcal{K}^{(n)}$ such defined guarantees

Algorithm 1 Construction of $\mathcal{K}^{(n)}$ defined in (11) by applying (8)-(9)

- 1: **Input:** $n \in \mathbb{N}$, $q : (0, 1) \rightarrow \mathbb{R}$
 - 2: **Output:** $\mathcal{K}^{(n)} \in \mathbb{R}^{n \times n}$
 - 3: Construct $\mathbf{q} := \left[q\left(\frac{1}{n+1}\right), \dots, q\left(\frac{n}{n+1}\right) \right]$
 - 4: Construct $Q^{(n)} = \text{diag}(\mathbf{q}) \in \mathbb{R}^{n \times n}$
 - 5: Construct $\Delta_{\infty, \text{dir}} = \text{toeplitz}(\mathbf{t}) \in \mathbb{R}^{n \times n}$, \mathbf{t} as in (10)
 - 6: Define $\mathcal{L}^{(n)} = n^2 \Delta_{\infty, \text{dir}} + Q^{(n)}$
 - 7: Compute U, Σ, V such that $\mathcal{L}^{(n)} = U \Sigma V^T$
 - 8: $\mathcal{K}^{(n)} = V \Sigma^\dagger U^T$
-

both (P1) and (P2'). We can check it numerically through an example. Let \mathcal{K} in (8) be characterized by

$$h(x, y) = \begin{cases} \sin^{-1}(1) \sin(1-x) \sin(y) & \text{if } 0 \leq y < x \leq 1, \\ \sin^{-1}(1) \sin(x) \sin(1-y) & \text{if } 0 \leq x \leq y \leq 1, \end{cases}$$

or, equivalently, let \mathcal{L} in (9) be characterized by $q(x) \equiv -1$. We want to compare the discretization $\mathcal{K}^{(n)}$ obtained by (11) with the discretization $\hat{\mathcal{K}}^{(n)}$ obtained by the Galerkin method with orthonormal box functions from (8). In Table I and Table II it is possible to check the validity of (P1) and (P2), respectively, for both the discretizations.

Table I

In this table we validate numerically the property (P1) for both the discretizations $\mathcal{K}^{(n)}$ and $\hat{\mathcal{K}}^{(n)}$. We choose the sup norm and $f(x) = x$ as test function. As it can be checked, the maximum absolute error tends to zero as n increases, for both the discretizations.

	Maximum Absolute Error		
	$n = 10^2$	$n = 10^3$	$n = 2 \cdot 10^3$
$\mathcal{K}^{(n)}$	4.8094e-04	4.8213e-05	2.4110e-05
$\hat{\mathcal{K}}^{(n)}$	0.0016	1.7749e-04	8.9109e-05

Table II

In this table we report the LSRE for both the discretizations $\mathcal{K}^{(n)}$ and $\hat{\mathcal{K}}^{(n)}$. As it can be checked numerically, the LSRE tends to zero as n increases for fixed m , for both the discretizations, therefore validating property (P2).

		LSRE		
		$n = 10^2$	$n = 10^3$	$n = 2 \cdot 10^3$
$\mathcal{K}^{(n)}$	$m = 1$	0.0053	5.3341e-04	2.6686e-04
	$m = 10$	0.0048	4.7988e-04	2.4007e-04
	$m = 50$	0.0048	4.7950e-04	2.3985e-04
$\hat{\mathcal{K}}^{(n)}$	$m = 1$	0.0100	9.9983e-04	4.9996e-04
	$m = 10$	0.0183	0.0011	5.2034e-04
	$m = 50$	0.1884	0.0031	0.0010

The difference between the two discretizations relies in Property (P2'). The eigenvalues of the continuous operator \mathcal{K} are given by $\lambda_m = \frac{1}{m^2 \pi^2 - 1}$, and Table III shows that $\mathcal{K}^{(n)}$ satisfies (P2') while $\hat{\mathcal{K}}^{(n)}$ fails it.

Table III

In this table we report the MSRE defined in (7), for the two discretizations $\mathcal{K}^{(n)}$ and $\hat{\mathcal{K}}^{(n)}$. As it can be checked numerically, the MSRE associated to $\mathcal{K}^{(n)}$ tends to zero as n increases while the MSRE associated to $\hat{\mathcal{K}}^{(n)}$ is stuck away from zero.

	MSRE			
	$n = 10^2$	$n = 5 \cdot 10^2$	$n = 10^3$	$n = 2 \cdot 10^3$
$\mathcal{K}^{(n)}$	0.0053	0.0011	5.3341e-04	2.6686e-04
$\hat{\mathcal{K}}^{(n)}$	0.3200	0.3098	0.3085	0.3078

To give a visual understanding of what happens, in Figure 1 we compare the eigenvalue distributions of $\mathcal{K}^{(n)}$ and $\hat{\mathcal{K}}^{(n)}$ with the eigenvalue distribution of \mathcal{K} . For a clear representation, we plotted the reciprocal of the first n eigenvalues normalized by n^2 .

IV. GRAPH LAPLACIAN AND THE PENALTY TERM

We build the operator $\mathcal{A}^{(n)}$, in the penalty term of (3), such that it can represent the graph Laplacian associated to a specific graph G that encodes informations from the observed data g^ϵ . A very common choice is the following, see for example [8], [20]: having fixed $n \in \mathbb{N}$, $r \in \{1, \dots, n\}$ and $\sigma > 0$, define $X = \left\{ x_i = \frac{i}{n+1} : i = 1, \dots, n \right\}$ and

$$w(x_i, x_j) = \begin{cases} e^{-\frac{(g^\epsilon(x_i) - g^\epsilon(x_j))^2}{\sigma^2}} & \text{if } |i - j| \leq r, \\ 0 & \text{otherwise.} \end{cases} \quad (12)$$

Then we write $\mathcal{A}^{(n)} := \Delta$, where Δ is the graph Laplacian (4) associated to $G = (X, w)$ just defined above, see Algorithm 2. The edge-weight function expresses the similarities between nodes, which (in this case) is given by a Gaussian distribution-like on the image-set of g^ϵ . This choice revealed to be fruitful in a recent work on image deblurring, see [5]. Indeed, the kernel of the graph Laplacian Δ , when the potential term κ is zero, is one-dimensional and its eigenspace is generated by the constant vector $[1, \dots, 1]$. Images typically are characterized by having wide portions of its area constituted by almost homogeneous color, and then it happens that

$$\|\Delta [f^\dagger]\| \approx 0,$$

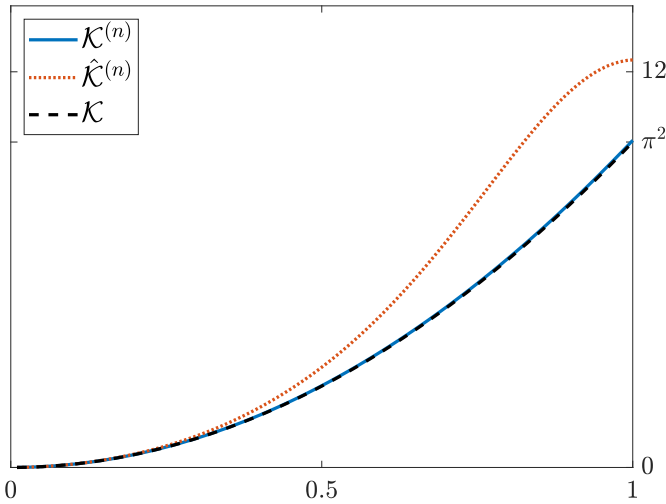


Figure 1. Graphical representation of (a suitable modification of) the first $n = 100$ eigenvalues associated to \mathcal{K} , $\hat{\mathcal{K}}^{(n)}$ and $\mathcal{K}^{(n)}$. We have plotted the reciprocal of their eigenvalues, normalized by n^2 and sorted in nondecreasing order. The continuous blue line and the continuous red line are associated to the modified eigenvalues of $\hat{\mathcal{K}}^{(n)}$ and $\mathcal{K}^{(n)}$, respectively. The dashed black line is associated to the modified eigenvalues of \mathcal{K} . On the x -axis is reported the ratio m/n , where m is referred to the m -th eigenvalue. As it can be seen, there is perfect match between the plots correspondent to \mathcal{K} and $\mathcal{K}^{(n)}$, while the plot correspondent to $\hat{\mathcal{K}}^{(n)}$ deviates consistently from \mathcal{K} in the mid-high frequencies. This behaviour confirms the results reported in Table III.

that is, f^\dagger “approximately” belongs to the kernel of Δ . Anyway, even if this approach generally can produce good results, there is still room for a great margin of improvement. Future lines of research have to concentrate on different w that can take into account other players, such as the operator \mathcal{K} itself, and a-priori informations regarding the true solution.

Algorithm 2 Construction of $\mathcal{A}^{(n)}$ in (3)

- 1: **Input:** $n \in \mathbb{N}$, $r \in \{1, \dots, n\}$, $\sigma > 0$, $\mathbf{g}_n \in \mathbb{R}^n$
- 2: **Output:** $\mathcal{A}^{(n)} \in \mathbb{R}^{n \times n}$
- 3: Construct $W \in \mathbb{R}^{n \times n}$ s.t. $(W)_{i,j} = w(x_i, x_j)$ as in (12)
- 4: Construct $\mathbf{d}_n \in \mathbb{R}^n$ s.t. $(\mathbf{d}_n)_i = \sum_{j=1}^n w(x_i, x_j)$
- 5: Construct $D = \text{diag}(\mathbf{d}_n) \in \mathbb{R}^{n \times n}$
- 6: Define $\Delta = D - W$
- 7: $\mathcal{A}^{(n)} = \Delta$

V. NUMERICAL EXAMPLES

In this section we provide some numerical examples of reconstructed solutions of the model problem (1) by means of the discretized version of the regularization operator (2a)-(2b), that is,

$$\mathbf{f}_{\alpha,n}^\epsilon := \mathcal{R}_\alpha^{(n)}[\mathbf{g}_n^\epsilon]$$

where $\mathcal{R}_\alpha^{(n)}$ is defined by (3). The continuous operator \mathcal{K} will be an integral operator of the form (8), and we are going to consider three model examples in the upcoming subsections. For all the examples, the matrix operator $\mathcal{A}^{(n)}$ in the penalty

term will be chosen among the identity matrix I and the following ones

$$\mathcal{A}_1^{(n)} = \begin{bmatrix} 2 & -1 & 0 & \cdots & 0 \\ -1 & 2 & -1 & & \\ & \ddots & \ddots & \ddots & \\ 0 & \cdots & 0 & -1 & 2 \end{bmatrix},$$

$$\mathcal{A}_2^{(n)} = \begin{bmatrix} 1 & -1 & 0 & \cdots & 0 \\ -1 & 2 & -1 & & \\ & \ddots & \ddots & \ddots & \\ 0 & \cdots & 0 & -1 & 1 \end{bmatrix},$$

and $\mathcal{A}_3^{(n)}$, given by Algorithm 2. Matrices $\mathcal{A}_1^{(n)}$ and $\mathcal{A}_2^{(n)}$ are the (normalized) discretization, by means of the 3-points Finite Difference method, of the one-dimensional Laplace operator on $(0, 1)$ with Dirichlet and Neumann BCs, respectively. The main operator $\mathcal{K}^{(n)}$ will be given by Algorithm 1, and its performance will be compared with a standard discretization by the Galerkin method with orthonormal box functions. We point out that the latter discretization do not satisfy (P2’).

All the computations are performed on MATLAB R2020b. The noisy data vectors \mathbf{g}_n^ϵ are obtained by adding Gaussian noise to the original data vectors \mathbf{g}_n and, in order to have repeatability of the numerical experiments, we fixed `rng(7)` for the function `randn()`. Specifically,

$$\mathbf{g}_n^\epsilon = \mathbf{g}_n + \epsilon \frac{\text{norm}(\mathbf{g}_n) \text{randn}(1, n)}{\text{norm}(\text{randn}(1, n))},$$

where ϵ is the noise level and n is the number of points that (uniformly) discretize the interval $(0, 1)$. The regularized solution $\mathbf{f}_{\alpha,n}^\epsilon$ is then obtained by applying the `tikhonov()` function which can be found in the `regtools` toolbox, see [14], and the goodness of the reconstruction is evaluated by computing the *relative restoration error* (RRE) in the ℓ^2 -norm,

$$\text{RRE} := \frac{\|\mathbf{f}_{\alpha,n}^\epsilon - \mathbf{f}_n^\dagger\|}{\|\mathbf{f}_n^\dagger\|}.$$

In this work we do not focus on the strategies for choosing the regularization parameters α, r, σ . In particular, r and σ , that appears in (12), can be difficult to set and ideally they should also be adapted to the noise level ϵ . For this reason, for all the numerical examples we fix $r = \lceil (0.2)n \rceil$ and $\sigma = 0.01$. The same goes for the α parameter: in all the experiments we choose the α that minimizes the RRE among fifty logarithmically spaced points between 10^3 and 10^{-6} .

A. Example 1

In this first example we consider as Green kernel the following function

$$h(x, y) = \begin{cases} y(x-1) & \text{if } 0 \leq y < x \leq 1, \\ x(y-1) & \text{if } 0 \leq x \leq y \leq 1, \end{cases}$$

which is the Green function of the operator (9), changed of sign and with $q(x) \equiv 0$. It is taken from the model problem `deriv2()` in the `regtools` toolbox. We consider the following test functions:

$$f_1^\dagger(x) = \begin{cases} [p_2^2(x) - p_3(x)]e^{4 - \frac{1}{p_1(x)}} & \text{if } (x - 1/2)^2 \leq 1/4, \\ 0 & \text{otherwise,} \end{cases}$$

where

$$p_1(x) := 0.25 - (x - 0.5)^2, \quad p_2(x) := 2 \frac{(x - 0.5)}{p_1^2(x)},$$

$$p_3(x) := \frac{2p_1^2(x)^2 + 8(x - 0.5)^2 p_1(x)}{p_1^4(x)};$$

and

$$f_2^\dagger(x) = \frac{x^3}{3} - \frac{x^2}{2}, \quad f_3^\dagger(x) = x, \quad f_4^\dagger(x) = e^x.$$

Some preliminary remarks: we choose f_1^\dagger because it belongs to $C_c^\infty(0,1)$, that is, the core subset of the operator (9), and f_2^\dagger because it satisfies Neumann BCs. Instead, f_3^\dagger and f_4^\dagger are test functions originally implemented in `deriv2()`.

In the first two tables, we present two unrealistic examples but that are enlightening. They provide an extreme and clear confirmation of the statements we did in the previous Sections III-IV. In Table IV, we choose f_1^\dagger and fixed $\epsilon = 0$: since $f_1^\dagger \in C_c^\infty(0,1)$, as we expected, a discretization of \mathcal{K} that better preserve all the spectrum improves dramatically the RRE. In Table V instead, we fixed $\epsilon = 0.1$ and assumed to know already the true solution f_3^\dagger , and we used this information to build a potential term κ to add to the graph Laplacian $\mathcal{A}_3^{(n)}$ such that $\mathcal{A}_3^{(n)} [f_{n,3}^\dagger] = 0$. Despite the high level of noise, the RRE is very low, as it can be compared with the results in Table VI, where a lower lever of noise is implemented. This is due to the fact that the true solution lives in the kernel of $\mathcal{A}_3^{(n)}$. It is interesting to notice how strong is the projection of the regularized solution $f_{\alpha,n}^\epsilon$ into the kernel of $\mathcal{A}_3^{(n)}$, so that the role of the discretization of \mathcal{K} becomes secondary.

Table IV

Toy-model example with f_1^\dagger and $\mathcal{A}^{(n)} = I$. The noise level is $\epsilon = 0$ and $n = 100$.

RRE	
$\mathcal{K}^{(n)}$	3.9195e-07
$\hat{\mathcal{K}}^{(n)}$	0.0187

Table V

Toy-model example with f_3^\dagger and $\mathcal{A}^{(n)}$ such that $\mathcal{A}^{(n)} [f_{n,3}^\dagger] = 0$. The noise level is $\epsilon = 0.1$ and $n = 100$.

RRE	
$\mathcal{K}^{(n)}$	0.0021
$\hat{\mathcal{K}}^{(n)}$	0.0024

In Table VI we provide the RRE for several combinations of $\mathcal{K}^{(n)}$, $\hat{\mathcal{K}}^{(n)}$ and $\mathcal{A}^{(n)}$. The first remark is that for every fixed operator $\mathcal{A}^{(n)}$ in the penalty term, the best RRE is given by using $\mathcal{K}^{(n)}$, for every f_i^\dagger . The second remark is that the best RRE is gained by the pair $\{\mathcal{K}^{(n)}, \mathcal{A}_3^{(n)}\}$, for all the test cases with the only exception of f_1^\dagger . In the test cases f_i^\dagger , for $i = 2, 3, 4$, the improvement is remarkable while in the test case f_1^\dagger the presence of $\mathcal{A}_3^{(n)}$ worsen drastically the RRE. This

is most probably due to the fact that the choice made for w in (12) does not fit well with functions that are compactly supported in $(0,1)$.

Table VI

For all these numerical experiments we fixed $\epsilon = 0.01$ and $n = 100$. In bold are highlighted the best RRE for each f_i^\dagger , $i = 1, 2, 3, 4$.

		RRE			
		I	$\mathcal{A}_1^{(n)}$	$\mathcal{A}_2^{(n)}$	$\mathcal{A}_3^{(n)}$
f_1^\dagger	$\mathcal{K}^{(n)}$	0.0836	0.0664	0.0869	0.2430
	$\hat{\mathcal{K}}^{(n)}$	0.0876	0.0686	0.0930	0.2416
f_2^\dagger	$\mathcal{K}^{(n)}$	0.2184	0.2275	0.0185	0.0176
	$\hat{\mathcal{K}}^{(n)}$	0.2262	0.2477	0.0308	0.0313
f_3^\dagger	$\mathcal{K}^{(n)}$	0.2017	0.1954	0.0391	0.0328
	$\hat{\mathcal{K}}^{(n)}$	0.2098	0.2258	0.0772	0.0678
f_4^\dagger	$\mathcal{K}^{(n)}$	0.1937	0.1912	0.0293	0.0089
	$\hat{\mathcal{K}}^{(n)}$	0.2021	0.2227	0.0453	0.0150

Finally, in Figure 2 we report the plots of the regularized solutions $f_{\alpha,n}^\epsilon$ from the test case f_4^\dagger in Table VI, for several different combinations.

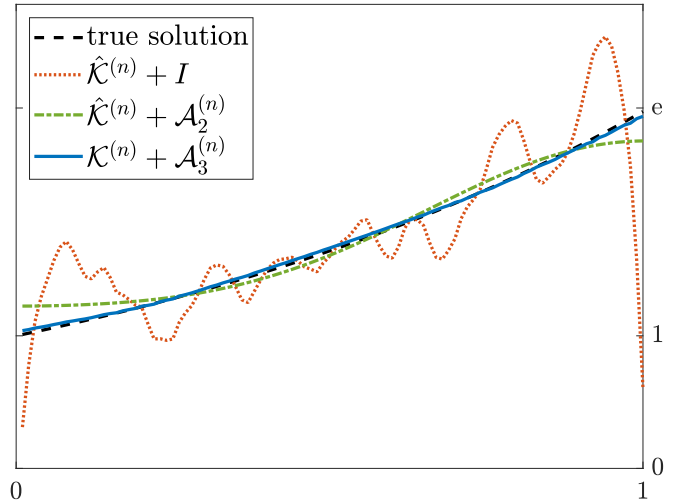


Figure 2. Plots of the regularized solutions $f_{\alpha,n}^\epsilon$ from the test case f_4^\dagger in Table VI, for several different combinations. The dashed-black line represents the true solution f_4^\dagger . The best RRE is achieved by the pair $\mathcal{K}^{(n)}$ and $\mathcal{A}_3^{(n)}$, that is represented by the continuous-blue line, and that can be easily checked by a direct visual inspection. Observe that if we choose $\mathcal{A}^{(n)} = I$ then $f_{\alpha,n}^\epsilon$ is forced to assume zero values at the endpoints $x = 0, x = 1$. This is due to the fact that \mathcal{K} is the Green operator associated to \mathcal{L} defined in (9), and $\text{dom}(\mathcal{L}) = H_0^1 = C_c^\infty(0,1)$.

B. Example 2

In this second example we take

$$h(x,y) = \begin{cases} \sin^{-1}(1) \sin(1-x) \sin(y) & \text{if } 0 \leq y < x \leq 1, \\ \sin^{-1}(1) \sin(x) \sin(1-y) & \text{if } 0 \leq x \leq y \leq 1, \end{cases}$$

as in Section III, and we keep the f_i^\dagger , for $i = 1, \dots, 4$ defined in the preceding Subsection V-A, as test functions. We collected the numerical results in Table VII, while in Figure 3

we provided the plots of the reconstructed solutions for the test case f_3^\dagger , for several different combinations of the discretized operator and the penalty term.

Table VII

For all these numerical experiments we fixed $\epsilon = 0.02$ and $n = 100$. In bold are highlighted the best RRE for each f_i^\dagger , $i = 1, 2, 3, 4$.

		RRE			
		I	$\mathcal{A}_1^{(n)}$	$\mathcal{A}_2^{(n)}$	$\mathcal{A}_3^{(n)}$
f_1^\dagger	$\mathcal{K}^{(n)}$	0.1202	0.0893	0.1133	0.4557
	$\hat{\mathcal{K}}^{(n)}$	0.1190	0.0905	0.1138	0.4636
f_2^\dagger	$\mathcal{K}^{(n)}$	0.2404	0.2185	0.0169	0.0161
	$\hat{\mathcal{K}}^{(n)}$	0.3330	0.3306	0.0636	0.0623
f_3^\dagger	$\mathcal{K}^{(n)}$	0.2637	0.2553	0.0426	0.0406
	$\hat{\mathcal{K}}^{(n)}$	0.3200	0.2908	0.1075	0.1003
f_4^\dagger	$\mathcal{K}^{(n)}$	0.2455	0.2395	0.0307	0.0116
	$\hat{\mathcal{K}}^{(n)}$	0.2937	0.2703	0.0900	0.0712

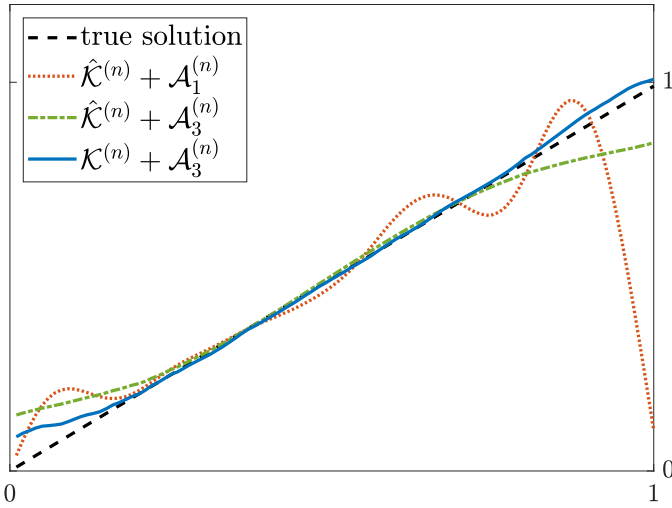


Figure 3. Plots of the regularized solutions $f_{\alpha,n}^\epsilon$ from the test case f_3^\dagger in Table VII, for several different combinations. The dashed-black line represents the true solution f_3^\dagger . The best RRE is achieved by the pair $\mathcal{K}^{(n)}$ and $\mathcal{A}_3^{(n)}$, that is represented by the continuous-blue line, and that can be easily checked by a direct visual inspection. Observe that if we choose $\mathcal{A}_1^{(n)}$ then $f_{\alpha,n}^\epsilon$ is forced to assume zero values at the endpoints $x = 0, x = 1$. This is due to the fact that $\mathcal{A}_1^{(n)}$ is a (normalized) discretization of \mathcal{L} defined in (9) for $q = 0$, and $\text{dom}(\mathcal{L}) = H_0^1 = \overline{C_c^\infty(0,1)}$.

VI. CONCLUSIONS

The main purpose of this short paper is to show that a good combination, of a discretization technique for the main operator \mathcal{K} and the operator \mathcal{A} in the penalty term, can improve by far the reconstructed solutions, if compared to some standard discretizations. We used a graph-based approach to both build $\mathcal{K}^{(n)}$ and $\mathcal{A}^{(n)}$, even if the two discretizations had different scopes. In the first case, we were interested to have a good spectral relative error all along the spectrum, in comparison with the spectrum of the real operator \mathcal{K} , while in the second case we wanted to find a good space

where to force into the reconstructed solution. The preliminary numerical results are promising, nevertheless there are still many open questions. For example, it is necessary to find a procedure to build a discretization of \mathcal{K} from the kernel h that guarantees $\mathcal{E} = 0$, without knowing the differential operator \mathcal{L} . Moreover, it has to be understood if all the spectrum should be preserved or if it is possible to concentrate on a smaller portion. Finally, the edge-weight function w , used to build the graph Laplacian $\mathcal{A}^{(n)}$ in the penalty term, should be refined such to encode more possible informations on the space where the true solution f^\dagger lives.

REFERENCES

- [1] H. C. Andrews, B. R. Hunt, *Digital image restoration*. Prentice-Hall, Englewood Cliffs, NJ (1977).
- [2] A. Adriani, D. Bianchi, S. Serra-Capizzano, *Asymptotic Spectra of Large (Grid) Graphs with a Uniform Local Structure (Part I): Theory*. Milan J. Math. 88(2) (2020): 409–454.
- [3] D. Bianchi, *Analysis of the spectral symbol associated to discretization schemes of linear self-adjoint differential operators*. Preprint (2020), arXiv:2004.10058.
- [4] D. Bianchi, M. Donatelli, *On generalized iterated Tikhonov regularization with operator-dependent seminorms*. ETNA 47 (2017): 73–99.
- [5] D. Bianchi, A. Buccini, M. Donatelli, E. Randazzo, *Graph Laplacian for image deblurring*. Preprint (2021), arXiv:2102.10327.
- [6] E. B. Davies, *Spectral theory and differential operators*. Cambridge University Press (1996).
- [7] A. Böttcher, S. M. Grudsky, *Toeplitz matrices, asymptotic linear algebra and functional analysis*. Vol. 67. Springer (2000).
- [8] L. Calatroni, Y. van Gennip, C. B. Schönlieb, H. M. Rowland, A. Flenner, *Graph Clustering, Variational Image Segmentation Methods and Hough Transform Scale Detection for Object Measurement in Images*. J. Math. Imaging Vis. 57(2) (2017): 269–291.
- [9] H. W. Engl, M. Hanke, A. Neubauer, *Regularization of inverse problems*. Vol. 375. Springer Science & Business Media (1996).
- [10] E. Estrada, *Path Laplacian matrices: Introduction and application to the analysis of consensus in networks*. Linear Algebra Appl. 436(9) (2012): 3373–3391.
- [11] E. Estrada, E. Hameed, N. Hatano, M. Langer, *Path Laplacian operators and superdiffusive processes on graphs. I. One-dimensional case*. Linear Algebra Appl. 523 (2017): 307–334.
- [12] W. N. Everitt, L. Markus, *Boundary value problems and symplectic algebra for ordinary differential and quasi-differential operators*. American Mathematical Soc. (1999).
- [13] C. W. Groetsch, *The theory of tikhonov regularization for fredholm equations*. Boston Pitman Publication (1984).
- [14] P. C. Hansen, *Regularization tools: a Matlab package for analysis and solution of discrete illposed problems*. Numer. Algorithms 6 (1994): 1–35.
- [15] T. K. Huckle, M. Sedlacek, *Tikhonov-Phillips regularization with operator dependent seminorms*. Numer. Algorithms 60 (2012): 339–353.
- [16] M. Keller, D. Lenz, *Dirichlet forms and stochastic completeness of graphs and subgraphs*. J. fur die Reine und Angew. Math. 666 (2012): 189–223.
- [17] M. Keller, D. Lenz, R. K. Wojciechowski, *Graphs and discrete Dirichlet spaces*. Grundlehrender mathematischen Wissenschaften: Springer, forthcoming (2021).
- [18] F. Lenti, F. Nunziata, C. Estatico, M. Migliaccio, *Spatial resolution enhancement of earth observation products using an acceleration technique for iterative methods*. IEEE Geosci. Remote Sensing 12 (2015): 269–273.
- [19] J. Lund, K. L. Bowers, *Sinc methods for quadrature and differential equations*. Society for Industrial and Applied Mathematics (1992).
- [20] G. Peyré, S. Bogleux, L. Cohen, *Non-local regularization of inverse problems*. In: Computer Vision – ECCV 2008, Springer Berlin Heidelberg, Eds D. Forsyth, P. Torr, A. Zisserman (2008): 57–68.